Submitted to ADVANCED MATERIALS
DOI: 10.1002/adma.((please add manuscript number))
Article type: Communication

Pancharatnam-Berry Phase Induced Spin-Selective Transmission in Herringbone Dielectric Metamaterials

Mitchell Kenney, Shaoxian Li, Xueqian Zhang, Xiaoqiang Su, Teun-Teun Kim, Dongyang Wang, Dongmin Wu, Chunmei Ouyang, Jiaguang Han, Weili Zhang, Hongbo Sun* and Shuang Zhang**

Mitchell Kenney and Shaoxian Li contributed equally to this work.

Dr. M. Kenney, Dr. T.-T. Kim, D. Wang, Prof. S. Zhang
School of Physics and Astronomy, University of Birmingham, B15 2TT, UK
E-mail: s.zhang@bham.ac.uk

Dr. M. Kenney
School of Engineering, Rankine Building, University of Glasgow, G12 8LT, UK

S. Li, Dr. X. Zhang, Dr. X. Su, D. Wang, Prof. C. Ouyang, Prof. J. Han, Prof. W. Zhang, Prof. S. Zhang
Center for Terahertz Waves and College of Precision Instrument and Optoelectronics Engineering, Tianjin University, Tianjin 300072, China
Email: cmouyang@tju.edu.cn

Dr. D. Wu
Key Laboratory of Nanodevices, Suzhou Institute of Nano-tech and Nano-bionics, Chinese Academy of Sciences, 398 Ruoshui Road, Suzhou, Jiangsu 215123, China

Prof. H. Sun
State Key Laboratory on Integrated Optoelectronics, College of Electronic Science and Engineering, Jilin University, 2699 Qianjin Street, Changchun 130012, China.
Email: hbsun@jlu.edu.cn

Keywords: (dielectric, metamaterials, metasurfaces, chirality, asymmetric transmission)

A key goal in the development of light-based systems is being able to accurately control the polarization of light. This is typically achieved with conventional polarizers and wave plates; however, this can involve optical setups with numerous cascaded components in addition to these being very bulky and not scalable to subwavelength sized devices, which will all contribute to a decrease of the efficiency and imaging quality. In the past decade or so, metamaterials have shown great promise in the controllability of light, to realize phenomena such as negative refraction,[1–4] zero refractive index,[5–7] invisibility cloaking,[8–10] and sub-

diffraction superlensing.[11–13] Even though metamaterials have been essential in developing new devices and a better insight into various fundamental physical laws, they still have not been adapted for real world applications. This is mainly due to the difficulties in fabrication and inherently low efficiency, which is a critical necessity in the ever growing requirement for lower energy consumption of devices. These issues are not trivial to overcome, with most metamaterials typically being composed of lossy metals, especially in the visible spectrum, and involving precise and time-consuming fabrication alignment processes, which is not an easy task even for the most state-of-the-art fabrication tools.

Recently, chiral metamaterials in the absence of mirror symmetry have been developed to invoke a chiral response, namely a contrast between the transmitted opposite spins of light. Most of these chiral metamaterials consist of 3D continuous helical structures[14,15] or stacked [16,17] metallic structures with twisted orientations. These 3D chiral structures (such as a helix) appear identical when viewed from both forward and backward directions and thus have equal responses for light. This in turn allows preferential transmission of one cross-polarization whilst prohibiting or reflecting the opposite one. Conversely, as detailed in the original work in Ref. [18] an anisotropic lossy planar chiral "fish-scale" structure was investigated and shown to exhibit Asymmetric Transmission (AT) (*alternatively known as Circular Conversion Dichroism (CCD))* for circularly polarized (CP) light in the microwave region, which was explained by the 'twist' vector **W** following the well-known 'cork-screw' law. Such a design appears reversed when viewed from opposite sides and so exhibits a directional response for the handednesses of CP light. This was then scaled down to work in the visible spectrum.[19] Similar works on using planar chiral metasurfaces were also carried out in the terahertz regime,[20] and for investigating broadband capabilities in the infrared (IR).[21] However, the chiral responses reported are usually very small for planar chiral metasurfaces. Recent methods have aimed to improve on this by utilizing aforementioned layered metasurfaces.[22,23]

However, these devices have very complex designs, involving time consuming optimizations of layer-to-layer distance and impedance matching, as well as difficult fabrication processes. In addition, these devices are still composed of lossy metals, and thus absorption losses are unavoidable (where in Ref. [23] losses are 37%).

Here, we present a new means of achieving a strong chiral response through a spin-selective interference between light of different Pancharatnam-Berry (PB) phases inside a birefringent metamaterial grating. The binary grating consists of a periodic arrangement of two uniaxial birefringent materials with the same anisotropy but an orientation angle difference of $\theta = \pi/4$ (each one forms a $\pi/8$ angle with respect to the symmetry line). The thickness of each of the birefringent materials satisfies the half wave plate condition such that a circularly polarized beam is completely converted to its opposite spin upon transmission. This spin flipping introduces a PB phase[24] such that the phase change of light introduced by an orientation angle θ between two structures is simply $\Phi = \pm 2\theta = \pm \pi/2$, with the + sign corresponding to RCP incidence/LCP transmission and the − sign corresponding to LCP incidence/RCP transmission. In addition, one structure is elevated with a certain thickness relative to the other such that a $\pi/2$ difference in the dynamic (propagating) phase between the two structures is introduced due to the different refractive indices between the substrate and the incident medium (air). Hence the overall phase difference between the two structures experienced by different handednesses of light is then

$$\Phi = \varphi_{Dyn} \pm \varphi_{PB} = \frac{\pi}{2} \pm \frac{\pi}{2} \quad (1)$$

which yields a total phase change of $\Phi = 0$ for LCP → RCP, and $\Phi = \pi$ for RCP → LCP. Therefore, RCP incident light undergoes destructive interference, *resulting in no LCP transmission and being completely reflected*, whilst LCP incidence has no overall phase change, corresponding to constructive interference and anti-reflection behaviour, *therefore allowing full*

transmission of converted RCP light. A diagram of the functional device is shown in **Figure 1c**. This novel approach is a simple yet effective method of achieving the aforementioned chiral response of CP light to yield a similar result as metallic chiral metasurfaces, yet only requiring dielectric materials.

It is well studied that subwavelength gratings can be utilized to exhibit birefringence,[25] whereby the incident light experiences both fast and slow axes dependent upon its polarization states (TE and TM). This introduces a form-birefringence to alter the polarization state of the transmitted light, due to the grating refractive indices n_{TM} and n_{TE}; the grating is then equivalent to a conventional birefringent crystal such as calcite, as a result of the effective medium approximation. By utilizing birefringence, the resulting analogy of the spin-selective metamaterial is given in **Figure 1a**, showing two identical birefringent crystals which are rotated such that the angle between their fast axes is $2\alpha = 45°$. A simplified schematic of the functionality of such a device is given in **Figure 1b**, where RCP incident light undergoes a phase change of π and therefore is not transmitted (only reflected), whilst an incident LCP wave is flipped and undergoes a phase change of 0π (or 2π) and therefore transmission is maximized. Such a functionality is then utilized via subwavelength (form-birefringent) gratings using silicon. This design has key advantages over the majority of previous methods used to achieve similar responses ─ the device is entirely made only of dielectric material, therefore Ohmic losses are negligible; fabrication is easily achieved by conventional plasma etching and photolithography; a simple and robust functionality is used, based on standard form-birefringent gratings in conjunction with geometric phase.

We investigated this effect at a frequency of 1 THz, within the so called "terahertz gap", as devices are of particular technological importance in this regime. To realize this, we chose to use silicon (Intrinsic, Ω = 10k Ohm, n = 3.418) which is transparent, has very low loss at THz frequencies, and is well studied for use in fabrication. The functionality of a subwavelength

device is dependent upon the period of the features being smaller than the wavelength of interest. For subwavelength gratings, the periodicity must satisfy the equation:

$$\Lambda \leq \lambda / n_{\mathrm{II}} \tag{2}$$

where n_{II} is the refractive index of the substrate material (and assuming that air is the background media $n_{\mathrm{I}} = 1$), Λ is the period of the gratings, and λ is simply the free space wavelength of interest. According to **Equation 2**, for a wavelength of 300 μm (corresponding to 1 THz) and the refractive index of silicon being $n_{\mathrm{Si}} = 3.418$, the periodicity of the gratings must be $\Lambda \leq$ 87.8 μm – to this end, we chose a periodicity of $\Lambda = 86$ μm. Providing that these gratings are subwavelength, the equation describing the depth and duty-cycle dependency of the phase accumulated by the light is given as:

$$\Delta\Phi_{TE-TM}(\lambda) = \left(\frac{2\pi h}{\lambda}\right) \Delta n_{form}(\lambda) \tag{3}$$

where h is the height/depth of the gratings (as shown in Figure 1c), λ is the free-space wavelength of the incident light, and $\Delta n_{form} = n_{TE}(\lambda) - n_{TM}(\lambda)$ is the difference between the refractive indices for light parallel (TE) or perpendicular (TM) to the gratings, respectively, which are given by:

$$n_{TE} = (F n_{\mathrm{I}}^2 + (1-F) n_{\mathrm{II}}^2)^{1/2} \tag{4}$$

$$n_{TM} = (F n_{\mathrm{I}}^{-2} + (1-F) n_{\mathrm{II}}^{-2})^{-1/2} \tag{5}$$

and F is simply the duty cycle of the gratings. Using the previously given refractive indices of air and silicon as $n_{\mathrm{I}} = 1$ and $n_{\mathrm{II}} = 3.418$, respectively, and a duty cycle of 0.5, we have that $n_{TE} = 2.52$ and $n_{TM} = 1.36$, respectively. We then obtain $\Delta n_{form}(\lambda) = 1.16$, such that when **Equation 3** is rearranged we obtain a grating depth of $h = 129\ \mu m$ (at a wavelength of $300\ \mu m$ and using a phase difference of $\Delta\Phi = \pi$) for the SWGs to function as half-wave plates. The schematic diagram of our device is shown in Figure 1c. We incorporate the PB Phase, to supply

the necessary handedness dependent π/2 phase shift, by having an angle of 45° set between the TM axes of two SWGs. The additional π/2 dynamic phase is introduced by an extra 'step' of silicon beneath one such grating, and is calculated using

$$\Delta\varphi_{Dyn} = \Delta n_{Si-Air}(2\pi d/\lambda) \tag{6}$$

where d is required to be 31 μm ($\Delta n_{Si-Air} = n_{\mathrm{Si}} - n_{\mathrm{Air}} = 2.418$). Incorporating all of these calculated dimensions together gives us our Monolithic silicon Herringbone patterned device.

To further support our theoretical predictions, a simplified analytical model based on Fresnel's equations for transmittance was employed. The system was considered to have three-layers – with layer 1 being air, layer 2 being an SWG, and layer 3 being bulk silicon. From this, we used the Fresnel equation for transmittance:

$$t_i = \frac{t_{12_i} t_{23_i} e^{-i\phi}}{1 + r_{12_i} r_{23_i} e^{-2i\phi}} \tag{7}$$

where i corresponds to x or y unit vectors, $t_{12_i} = 2n_1/(n_1 + n_{2i})$, $t_{23_i} = 2n_{2i}/(n_{2i} + n_3)$, $r_{12_i} = (n_1 - n_{2i})/(n_1 + n_{2i})$, $r_{23_i} = (n_{2i} - n_3)/(n_{2i} + n_3)$, and $\phi_i = \frac{2\pi d}{\lambda} n_{2i}$, where d is the thickness of the SWG (layer 2). Once the circular Jones components for a single SWG are obtained, we then introduce the geometric (PB) and dynamic phase accumulations through a second identical SWG. The total transmitted intensity of the two SWG's combined is then given as:

$$T = n_3 \left| \frac{1}{2} t\left(1 + e^{i(\phi_{Dyn} + \phi_{PB})}\right) \right|^2 \tag{8}$$

with t corresponding to any of the circular Jones matrix components for the SWG (t_{RR}, t_{LL}, t_{LR}, t_{RL}), ϕ_{Dyn} is simply the dynamic phase from **Equation 6**, and ϕ_{PB} is the geometric phase equal to ± π / 2 (depending on the cross-polarization component) arising from the angular disparity of the two SWG's (ϕ_{PB} = 0 for both t_{RR} and t_{LL}). The calculated frequency dependent response

of the transmitted intensities are shown in **Figure 2a**. The values of *d* and *h,* as shown in Figure 1c, were set to 31 μm and 129 μm, respectively, as required for optimal functionality. A very clear difference between both T_{RL} and T_{LR} components can be seen, where the intensity of T_{RL} exceeds 85% transmittance whilst T_{LR} is negligible and has a value of zero transmittance at 1.0THz, as required. There is a slight difference between the frequencies at which the destructive (T_{LR}, $\Phi = \pi$) and unaffected (T_{RL}, $\Phi = 0$) beams occur, with $T_{LR} = 0$ occurring at the expected frequency of 1.0 THz whilst the T_{RL} maxima occurs at ~1.1 THz. This discrepancy can be attributed to the half-wave plates' (being approximated as SWG's) form-birefringence arising from the First Order effective medium theory, rather than using a higher order formulation.[26] Additionally, the intuitive single-pass formulation does not take into consideration the interfacial aspects of the complete structure; hence, Fabry-Pérot resonance effects resulting from the reflectance terms in the denominator of **Equation 7** lead to the analytical transmittances differing from the simple phase-only predictions of **Equation 1**.

In order to reinforce the theoretical reasoning and functionality of our device, full wave simulations were carried out using the commercially available *CST Microwave Studio* software package. The results of the circular transmission components are shown in **Figure 2b**. As can be seen, the results show a very good correspondence to those for the analytical model, especially apparent for T_{RL} exceeding a transmittance of 85% at 1.05 THz, and also show a clear difference between the cross-polarization components of T_{RL} and T_{LR}. One discrepancy that is worth noting is that the device can no longer be considered as subwavelength for frequencies much larger than the operational frequency of ~1 THz, and would result in diffraction occurring causing spurious interference effects. Transmission and phase information comparing the operation of an analogous bulk birefringent media to a grating is given in the Supplementary material, through numerical simulations with CST, in order to confirm the half-wave plate operation.

To experimentally verify our theoretical reasoning, the structure shown in Figure 1c was fabricated by conventional photolithography and Deep Reactive Ion Etching (DRIE) using a two-step pattern process (details provided in the Experimental Section). The complete fabricated device is shown in **Figure 3**, imaged using a Scanning Electron Microscope (SEM). The measured geometry of the fabricated structure slightly differs to the ideal geometry; it is visible from the Inset of Figure 3 that the top 'step' is larger than the bottom 'step', due to the decreased etch rate at the bottom of the trenches. As such, the top step is as designed, at 31 μm, whilst the bottom step is only 20 μm, which is a 35% difference in size. To establish the effect this has on the performance and functionality, simulations were carried out to reflect these different dimensions as shown in **Figure 4a**. It is clear that by comparing Figure 4a and Figure 2b we see very little difference in the transmission coefficient responses, with especially little difference to the curve for $T_{RL.}$ Therefore, we can assume that the device will be highly robust to fabrication variations and even a 35% change in the desired step height does not significantly affect the physical response.

To characterize and obtain the transmission data for our device, a fiber-based Terahertz Time-Domain Spectroscopy (THz-TDS) system is used to measure linear Jones matrix components ($T_{xx}, T_{yy}, T_{xy}, T_{yx}$) of the herringbone structure at normal incidence for a frequency range of 0.2 - 2.0 THz, which can be converted into the transmission matrix in the circularly polarized basis. The results for the experimental data characterisation are shown in **Figure 4b**. It is clear that there is indeed an asymmetry between the T_{RL} (red) and T_{LR} (blue) components as expected. The frequency of highest conversion occurs at 1.025 THz, which is very close to the design frequency of 1 THz. Here, the value of T_{RL} is 0.62, which indicates that 62% of LCP light incident onto the structure is converted into the opposite handedness of RCP. Conversely, T_{LR} gives a value of only 0.13. The extinction ratio between T_{RL} and T_{LR} is then approximately 5:1, which is very close to the performance of that for the simulation. Although the performance

of 62% for T_{RL} is not quite the 85% as was achieved in the simulation, this result is still remarkable given that the structure is a single layer and purely dielectric. The discrepancy can be attributed to the non-negligible material losses and scattering which may occur, as well as fabrication errors. At this central frequency of 1.025 THz, a FWHM of 0.72 THz is achieved which is again very broadband, although not as much as that for the simulation. Examining the total energy of the device for both RCP and LCP incident handednesses, we get values of $T_R = 0.28$ and $T_L = 0.84$. Such a result is significant in the sense that this device can be used to distinguish the circular handedness of incident light to a very high efficiency from either transmission or reflection modes.

In conclusion, we have demonstrated and fabricated a functional monolithic dielectric device to achieve a strong asymmetry between the orthogonal circular polarizations of transmitted light, which provides a very high broadband capability and transmittance of one cross-polarization whilst prohibiting the opposite one. Impressively, the herringbone metasurface not only provides an experimental cross-polarization transmittance of 0.62 for T_{RL}, but also has a greater transmittance than pure silicon alone or any other similar works carried out using planar metasurfaces to achieve a chiral response. Due to the lack of metallic structures, losses are negligible and the application of subwavelength gratings in conjunction with a geometric phase provides a robust and novel means of achieving such a functionality, which may provide a preferable route for optical computing or image processing where the demand on high efficiency is crucial.

Experimental Section

Simulations: The numerical simulations were carried out by using the commercially available Matlab and CST Microwave Studio (CST MWS) softwares. Matlab was used for plotting the frequency response of the analytically derived transmission coefficients. CST MWS was used

to perform time-domain solver calculations of the herringbone device, where periodic boundary conditions were chosen for each unit cell in the *x* and *y* directions, whilst the *z* direction was set as open. Linearly polarized light was used, and the corresponding *x* and *y* response amplitudes and phases were utilized to calculate the circularly polarized response (using the equations from Ref. [27]).

Sample Fabrication: Conventional photolithography and DRIE processes were used to fabricate the herringbone metamaterial. A 525μm intrinsic silicon wafer (<100>, Ω = 10,000 Ohm, n = 3.418) was cleaned and a 7-8 um thick AZ4620 photoresist spun onto it. This was then exposed to a stripe pattern photomask (with stripe periodicity of W, Figure 1c), fill factor 0.5, using a Karl Suss MA6 Mask Aligner for 16s (145 mJ/cm^2) and then developed. Following this, a DRIE (Bosch) process was used to etch the stripe pattern into the wafer to a depth of 30μm (corresponding to 'd' from Figure 1c). The remaining AZ4620 photoresist was then removed, and the sample thoroughly cleaned in acetone and IPA. Next, a 50μm thick layer of SU8-2050 photoresist was spun (at 4000RPM) onto the stripe-etched wafer (the 50μm thickness is a necessity to provide a planarized top surface which has 20um thickness above the top of the stripe trenches). The SU8-2050 is then exposed to a "zig-zag" patterned photomask using the MA6 for 20s (180 mJ/cm^2), followed by 5 minutes post-exposure baking at 95°C, and then developed for 7 minutes. This "zig-zag" patterned wafer is then etched using DRIE (Bosch) process for 130μm into the silicon (corresponding to 'h' from Figure 1c). Due to the very robust nature of SU8-2050, removal had to be done using multiple piranha (H_2SO_4:H_2O_2 mixture) cleans, and an O2 RIE process to assure that all of the SU8 had been removed.

Measurements: Samples were characterized at normal incidence using a THz-TDS system, comprising of a pair of commercial fiber-based THz photoconductive switches (MenloSystems) as transmitter and receiver. A set of 4 wire-grid polarizers were used to obtain the circular Jones

matrix components, where P1 and P4 were aligned parallel to each other, whilst P2 and P3 (where P1, P2 are situated before the metamaterial, and P3, P4 are situated after the metamaterial, respectively) were set at 45° to P1 and P4. P2 and P3 are allowed to change between + and – 45°, independently, such that cross polarization values can be obtained. A set of four 90° off-axis parabolic mirrors is used, where M1 (positioned after the source) is used to collimate the THz beam incident into the polarizers P1, P2. Another mirror (M2) placed after the polarizers is used to focus onto the sample, and a mirror after the sample (M3) is used to re-collimate the beam through polarizers P3, P4. Following this, a final mirror (M4) is then used after the polarizers to focus the beam onto the signal.

Supporting Information
Supporting Information is available online from the Wiley Online Library or from the author.

Acknowledgements

This work was financially supported by ERC Consolidator grant (TOPOLOGICAL), Leverhulme (grant no. RPG-2012-674) and the Opened Fund of the State Key Laboratory on Integrated Optoelectronics (IOSKL2014KF12).

Received: ((will be filled in by the editorial staff))
Revised: ((will be filled in by the editorial staff))
Published online: ((will be filled in by the editorial staff))

[1] J. B. Pendry, *Phys. Rev. Lett.* **2000**, *85*, 3966.

[2] R. A. Shelby, D. R. Smith, S. Schultz, *Science* **2001**, *292*, 77.

[3] S. Zhang, W. Fan, N. C. Panoiu, K. J. Malloy, R. M. Osgood, S. R. J. Brueck, *Phys. Rev. Lett.* **2005**, *95*, 137404.

[4] V. M. Shalaev, W. Cai, U. K. Chettiar, H.-K. Yuan, A. K. Sarychev, V. P. Drachev, A. V. Kildishev, *Opt. Lett.* **2005**, *30*, 3356.

[5] M. Silveirinha, N. Engheta, *Phys. Rev. Lett.* **2006**, *97*, 157403.

[6] A. Alù, M. G. Silveirinha, A. Salandrino, N. Engheta, *Phys. Rev. B* **2007**, *75*, 155410.

[7] X. Huang, Y. Lai, Z. H. Hang, H. Zheng, C. T. Chan, *Nat. Mater.* **2011**, *10*, 582.

[8] D. Schurig, J. J. Mock, B. J. Justice, S. A. Cummer, J. B. Pendry, A. F. Starr, D. R. Smith, *Science* **2006**, *314*, 977.

[9] J. Valentine, J. Li, T. Zentgraf, G. Bartal, X. Zhang, *Nat. Mater.* **2009**, *8*, 568.

[10] T. Ergin, N. Stenger, P. Brenner, J. B. Pendry, M. Wegener, *Science* **2010**, *328*, 337.

[11] N. Fang, H. Lee, C. Sun, X. Zhang, *Science* **2005**, *308*, 534.

[12] T. Taubner, D. Korobkin, Y. Urzhumov, G. Shvets, R. Hillenbrand, *Science* **2006**, *313*, 1595.

[13] Z. Liu, H. Lee, Y. Xiong, C. Sun, X. Zhang, *Science* **2007**, *315*, 1686.

[14] J. K. Gansel, M. Thiel, M. S. Rill, M. Decker, K. Bade, V. Saile, G. von Freymann, S. Linden, M. Wegener, *Science* **2009**, *325*, 1513.

[15] J. K. Gansel, M. Wegener, S. Burger, S. Linden, *Opt. Express* **2010**, *18*, 1059.

[16] A. V. Rogacheva, V. A. Fedotov, A. S. Schwanecke, N. I. Zheludev, *Phys. Rev. Lett.* **2006**, *97*, 1.

[17] M. Decker, M. W. Klein, M. Wegener, S. Linden, *Opt. Lett.* **2007**, *32*, 856.

[18] V. A. Fedotov, P. L. Mladyonov, S. L. Prosvirnin, A. V. Rogacheva, Y. Chen, N. I. Zheludev, *Phys. Rev. Lett.* **2006**, *97*, 167401.

[19] A. S. Schwanecke, V. A. Fedotov, V. V. Khardikov, S. L. Prosvirnin, Y. Chen, N. I. Zheludev, *Nano Lett.* **2008**, *8*, 2940.

[20] R. Singh, E. Plum, C. Menzel, C. Rockstuhl, A. K. Azad, R. A. Cheville, F. Lederer, W. Zhang, N. I. Zheludev, *Phys. Rev. B* **2009**, *80*, 153104.

[21] C. Pan, M. Ren, Q. Li, S. Fan, J. Xu, *Appl. Phys. Lett.* **2014**, *104*, 121112.

[22] L. Wu, Z. Yang, Y. Cheng, M. Zhao, R. Gong, Y. Zheng, J. Duan, X. Yuan, *Appl. Phys. Lett.* **2013**, *103*, 021903.

[23] C. Pfeiffer, C. Zhang, V. Ray, L. J. Guo, A. Grbic, *Phys. Rev. Lett.* **2014**, *113*, 023902.

[24] X. Chen, L. Huang, H. Mühlenbernd, G. Li, B. Bai, Q. Tan, G. Jin, C.-W. Qiu, S. Zhang, T. Zentgraf, *Nat. Commun.* **2012**, *3*, 1198.

[25] C. Delacroix, P. Forsberg, M. Karlsson, D. Mawet, O. Absil, C. Hanot, J. Surdej, S. Habraken,

Appl. Opt. **2012**, *51*, 5897.

[26] P. Lalanne, J.-P. Hugonin, *J. Opt. Soc. Am. A* **1998**, *15*, 1843.

[27] C. Menzel, C. Rockstuhl, F. Lederer, *Phys. Rev. A* **2010**, 82, 053811.

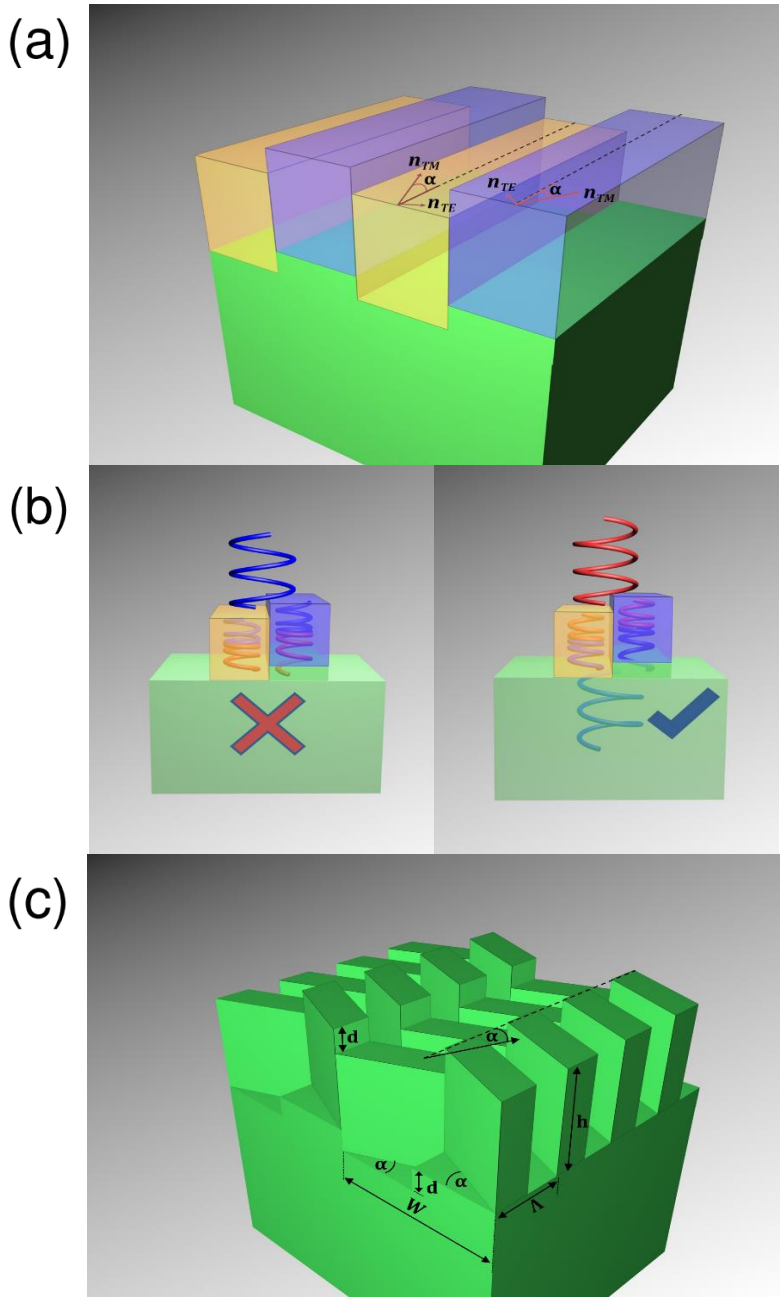

Figure 1. (a) Analogous representation of the herringbone device functionality, composed of homogeneous birefringent crystals with an angle of 45° between their fast axes (TM). **(b)** Schematic of the device functionality for RCP (blue) and LCP (red) incident light. For RCP incidence, an overall phase of π is obtained, and limits transmission (only reflection), whilst for LCP incidence the overall phase is 0 (or 2π) and the transmitted light is flipped. **(c)** The monolithic silicon herringbone device and corresponding dimension parameters, where $\Lambda = 86\mu m$, $d = 31\mu m$, $W = 208\mu m$, $h = 129\mu m$, and $\alpha = 22.5$.

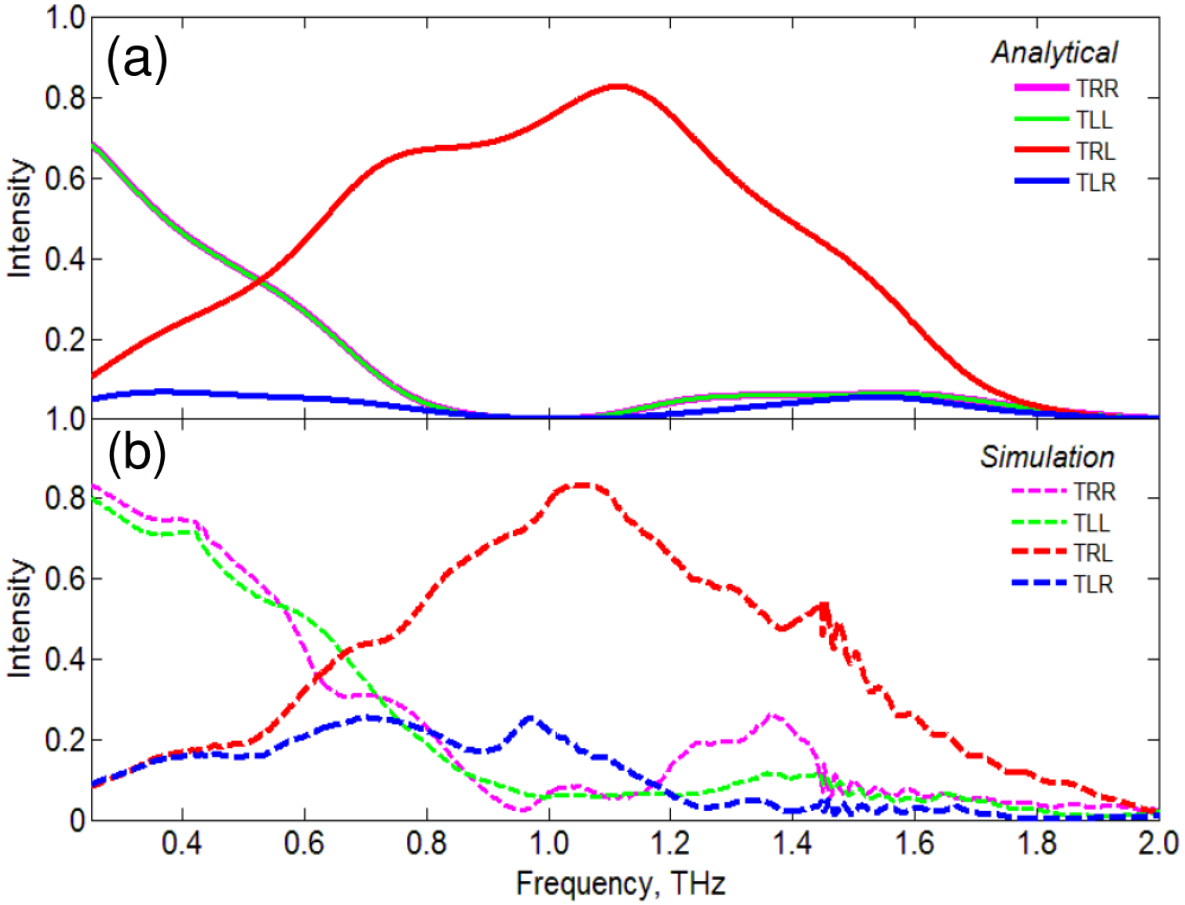

Figure 2. (a) The analytically derived transmission responses for the Jones matrix in a circular basis. **(b)** Simulated circular Jones matrix responses for the dimensions given in Figure 1c for the herringbone device.

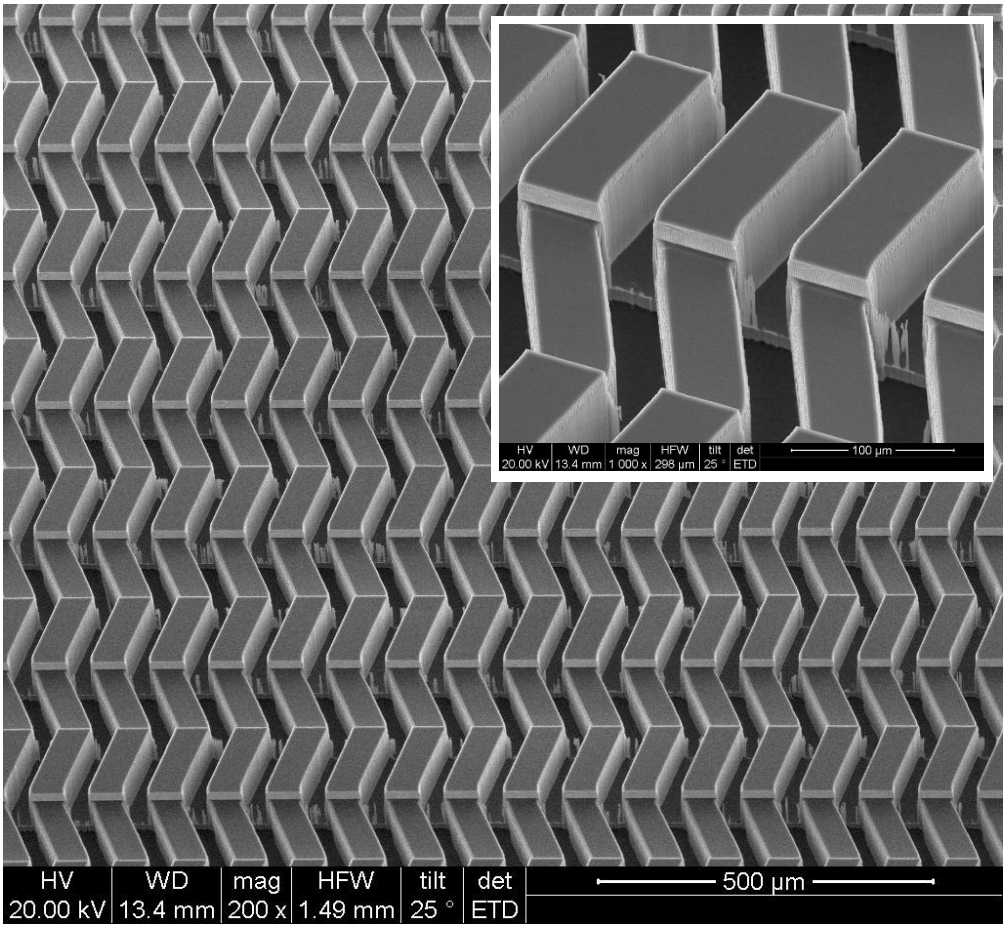

Figure 3. Scanning Electron Micrograph of the fabricated silicon herringbone device. **Inset**: Zoomed in Scanning Electron Micrograph showing the well-defined structures.

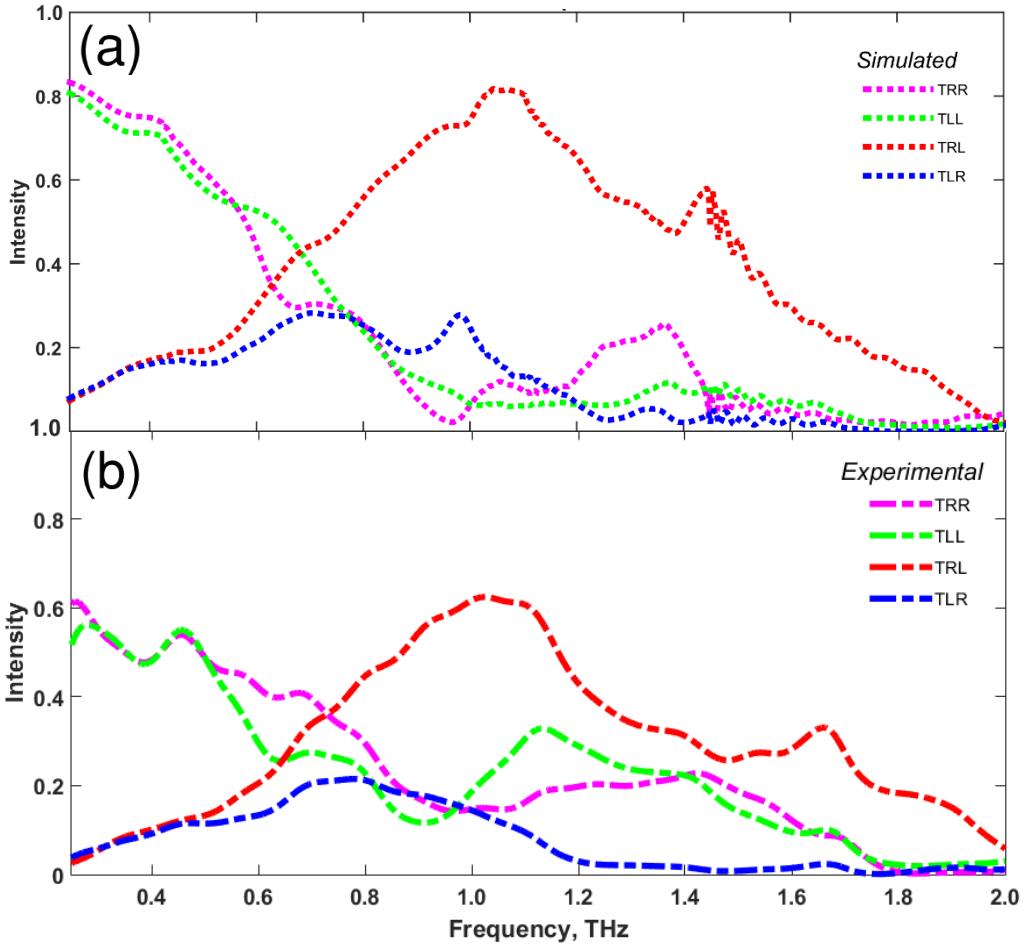

Figure 4. (a) Simulated responses of the device when using the dimensions of the fabricated device. **(b)** Experimentally obtained transmission coefficients from a THz-TDS system. The results are normalized to bare silicon.

The table of contents entry should be 50−60 words long (max. 400 characters), and the first phrase should be bold. The entry should be written in the present tense and impersonal style.

We propose a dielectric metamaterial approach for achieving spin-selective transmission of electromagnetic waves. The design is based on a spin-controlled constructive or destructive interference between propagating phase and Pancharatnam-Berry phase. The dielectric metamaterial, consisting of monolithic silicon herringbone structures, exhibits a broadband operation in the terahertz regime.

Keyword (Metamaterials; Metasurfaces; Pancharatnam-Berry Phase; Geometric Phase; Circular Dichroism)

Mitchell Kenney, Shaoxian Li, Xueqian Zhang, Xiaoqiang Su, Teun-Teun Kim, Dongyang Wang, Dongmin Wu, Chunmei Ouyang*, Jiaguang Han, Weili Zhang, and Shuang Zhang*

Pancharatnam-Berry Phase Induced Spin-Selective Transmission in Herringbone Dielectric Metamaterials

ToC figure ((Please choose one size: 55 mm broad × 50 mm high **or** 110 mm broad × 20 mm high. Please do not use any other dimensions))

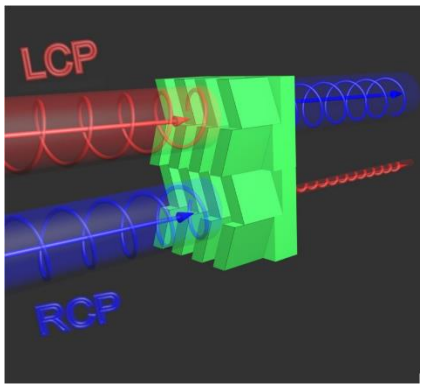

((Supporting Information can be included here using this template))

Supporting Information

for *Adv. Mater.*, DOI: 10.1002/adma.201603460

Pancharatnam-Berry Phase Induced Spin-Selective Transmission in Herringbone Dielectric Metamaterials

*Author(s), and Corresponding Author(s)** ((write out first and last name))

((Please insert your Supporting Information text/figures here. Please note: Supporting Display items, should be referred to as Figure S1, Equation S2, etc., in the main text…)